3.4 LIDAR OBSERVATION OF JET ENGINE EXHAUST FOR AIR QUALITY

Wynn L. Eberhard* and W. Alan Brewer
NOAA Environmental Technology Laboratory

Roger L. Wayson
University of Central Florida

1. INTRODUCTION

The exhaust from jet engines on aircraft is one source of air pollution (Fig. 1). Section 2 summarizes the pertinent characteristics of the jet engine exhaust plumes. This paper discusses two ways in which lidar can contribute to understanding the air quality effects from these emissions. One is measurement of the initial growth of the exhaust plume due to high velocity and shear and rise due to its elevated temperature. We observed the behavior of jet engine exhaust plumes from many aircraft during the first few tens of seconds after they commenced takeoff roll by detecting enhanced backscatter from particles emitted by the engines. The lidar system, sampling strategy, and analysis are described in Sections 3 and 4. The results are being used as input to at least one air quality model.

Fig. 1. Particulates in the exhaust of an aircraft just after take off.

Secondly, the potential for using lidar to determine the emission rates of soot from aircraft engines is addressed is Sections 5-7. Soot emissions contribute to the PM2.5 in the area of airports. During our measurements of plume geometry it was obvious that newer-generation aircraft on the whole produced less backscatter. This would seem to correspond with the aircraft industry's attempts to make engines more efficient and less polluting. The lidar also tended to detect stronger signal when the exhaust plume was obvious to the eye. This experience suggested that a calibrated lidar might be able to remotely infer soot concentrations and emission rates from aircraft jet engines. Soot measurements have been performed *in situ* (D. W. Fahey and U. Schumann in IPCC 1999 pp. 72-76), some on the ground (e.g. Hagen et al. 1992, Petzold et al. 2003, Nyeki et al. 2004) and others at altitude by chase aircraft (e.g., Hagen et al. 1996, Petzold et al. 1999). Petzold et al. (1999) estimated the emission index of soot EI_m (mass emitted per mass fuel consumed) of the world's fleet of aircraft to be 0.04 g kg^{-1}, but the uncertainty in this is a factor of 2 at best (J. S. Lewis and R. W. Niedzwiecki in IPCC 1999 p. 236). Aircraft operating on or near the ground at airports experience a wide range of power settings and less than optimal conditions for jet engines, so emission rates that impact air quality are poorly known. A remote sensing method that could relatively inexpensively observe soot emissions from many types of aircraft over their range of operating conditions could greatly reduce this uncertainty.

2. CHARACTERISTICS OF JET ENGINE EXHAUST

A brief description of the characteristics of jet engine exhaust provides the context for discussion of lidar measurements. Compressor blades in the front of jet engines compress the intake air. The air enters the combustor section where it is mixed with fuel and burns. Many commercial aircraft engines have turbofan engines in which most of the intake air passes to the side of the combustor. The exhaust from the combustor directly drives the turbine, indirectly drives the compressor through gearing, and, in the case of turbofan engines, drives the large fan that is responsible for most of the thrust. The thrust of hot gas out the exit nozzle also helps propel the aircraft forward. The initial exhaust has a core of hot, high-velocity gas from the combustor, coaxially surrounded by lower-speed bypass air.

Fuel burning combines the carbon and hydrogen atoms in the fuel with oxygen to generate energy and in the process forms H_2O and CO_2. The combustor exhaust contains particles of carbon, unburned fuel, and inorganic matter that was also present in the fuel. The carbon, or soot, is the primary non-volatile component, but the exhaust also contains other nonvolatiles including metals, sulfates, and nitrates.

The exhaust plume grows in crosswise dimension, and the velocity of the air in it decreases with distance behind the engine. The temperature difference between the exhaust and the ambient air is thought to be the

Corresponding author address: Wynn L. Eberhard, R/ETL2-NOAA, U.S. Dept. of Commerce, 325 Broadway, Boulder CO 80305; 303-497-6560; e-mail: wynn.eberhard@noaa.gov.

primary reason for plume rise. The push of exhaust air against the ambient air and turbulence generated by velocity shear contribute to this expansion. The turbulence causes some mixing of the combustor exhaust, bypass air, and ambient air. The air velocity in the plume depends mainly on the distance behind the aircraft, the thrust of the engines, and the aircraft speed. Speeds that are significantly higher than the motion of the ambient air can extend several hundred meters behind a large aircraft at takeoff power.

The temperature of the exhaust plume decreases with distance behind the engine through radiation, expansion, and mixing with ambient air. At any distance, the per cent difference of plume temperature compared to ambient temperature in degrees Kelvin is typically much less than the % difference of exhaust air speed compared to ambient wind speed.

As the plume ages, the volatile components, such as hydrocarbons, also begin to create small aerosol particles. Deposition of sulfuric acid and hydrocarbons on the soot particles also takes place, increasing their mass to some extent. Some of the particles coagulate, forming larger particles from multiple smaller ones.

3. LIDAR DESCRIPTION

A lidar transmits a pulse of light, which undergoes scattering and absorption as it propagates away from the system. A small part of the scattered light travels straight back to the lidar, where it is gathered and focused by a telescope onto a detector. The detector voltage is digitized as a function of time, and recorded as a function of range from the lidar.

After calibration and other factors are applied, the lidar signal can be expressed as

$$P = C\left[\beta_p(R)+\beta_m(R)+\beta_a(R)\right] \times exp\left\{-2\int_0^R \left[\sigma_p(R')+\sigma_m(R')+\sigma_a(R')\right]dR'\right\} \quad (1)$$

where C is the calibration factor, R is range, β is volumetric differential backscatter cross-section, σ is volumetric extinction coefficient, and subscripts p, m, and a refer to particles in the exhaust plume, air molecules, and ambient aerosol particles, respectively. Both scattering and absorption contribute to the extinction coefficient.

The laser we selected for jet exhaust measurements was a Nd:YAGx3 transmitting at 355-nm wavelength. Eyesafe operation was easy to achieve in the ultraviolet with simple precautions. The light is invisible, so there was no interference with pilot vision night or day. When the beam strikes a hard target it fluoresces about as brightly as if illuminated by a small penlight, so it is best to keep the beam scanning at night to avoid raising the curiosity of the public as well as help ensure eyesafety. The 355-nm wavelength is also close to optimum for detecting the particles in the jet exhaust in the presence of scattering from molecules and from ambient particles. We used our OPAL (Ozone Profiling Atmospheric Lidar, Fig. 2), but operated only with the "aerosol channel" (Table 1). The lidar could scan in elevation angle but had a fixed azimuth. Real-time data displays (Fig. 3) helped the experimenters optimize sampling strategy, but raw data were recorded on DAT tapes.

Fig. 2. Lidar system for plume geometry measurements. The enclosure on top contained the elevation-scanning mirror.

Parameter	Value
Wavelength	355 nm
Pulse energy	8 mJ
Pulse repetition rate	10 s^{-1}
Pulse length	10 ns
Range gate length	5 m
Telescope diameter	0.2 m
Elevation angle resolution	0.2°

Table 1. Specifications of lidar used for plume geometry measurements.

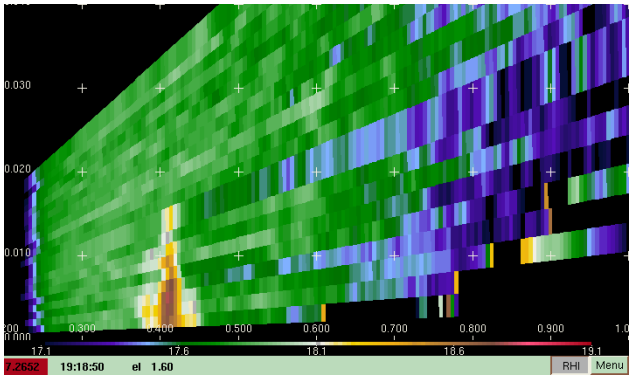

Fig. 3. Example false color display of backscatter from the ambient air (greens) and a jet exhaust (browns). The vertical scale is expanded about 10 times more than the horizontal.

4. EXHAUST PLUME GROWTH AND RISE

The lidar observed plume geometry during 17-24 May 2001 at Los Angeles International Airport. The lidar was positioned about 400 m from Runway 25R and scanned in a vertical plane oriented nearly

perpendicular to the runway centerline. Data acquisition began as each aircraft commenced takeoff roll and passed through the scan plane. The lidar automatically repeated vertical sweeps until the operator halted data acquisition because of poor data quality. Causes for degradation of data quality included loss of contrast against the signal from the ambient air, growth of the plume so the top of the plume obviously rose above the top of the scan, or the next aircraft reached the scan plane. Each sweep lasted about 5 s.

The majority of the aircraft generated plumes with adequate contrast, and these were used in the ensuing analysis. Other aircraft created very weak or invisible plumes relative to ambient. This did not mean particle emissions were zero, but rather that the backscatter from the emitted particles was about the same as from the ambient air. Some plumes in very hazy conditions were "negative", i.e., had less backscatter than the ambient. This was presumably caused by a combination of volatilization of the ambient particles passing through the engine and low particle emissions. Measurements were performed on more than 900 aircraft, and 4138 sweeps for 359 aircraft were retained after initial processing and quality control. Plumes from 21 types of aircraft were successfully detected.

Video cameras recorded the scan area to document aircraft position and the time the aircraft commenced takeoff roll. Binocular-equipped spotters reported aircraft type, airline, and tail number to the operator, who recorded these in the log sheet. These data were later matched with departure logs obtained from the airport to ensure accuracy and to identify the type of aircraft when tail numbers were not available at night.

The first stages of lidar data postprocessing used common methods. DC signal levels from background light and electronic offsets were removed based on pretrigger data. Adjustments for the pulse energy monitor and the range-squared correction were applied, producing P as given in (1).

The remainder of the processing was designed to reveal the geometry of the plume. Data from each sweep were displayed in range-angle coordinates with an approximate value of $\sigma_m + \sigma_a$ applied to flatten out the signal in range, and an analyst selected the sweeps with adequate data for further processing. Data from each selected sweep were displayed again later, and the analyst designated three regions in range: the range gates containing the enhanced signal from the jet engines (plume region), ~20 range gates with signal from ambient air closer to the lidar (near region), and ~20 range gates with signal from ambient air on the far side of the plume (far region). Extinction by plume particles and along-beam inhomogeneity in the ambient aerosol were approximately compensated by finding the ratio of the average signal in each of the near and far regions and applying an average "extinction coefficient" through the plume region to make the far region average the same as in the near region. This procedure is not mathematically rigorous, but it accounted for natural conditions in a simple and effective way for revealing the plume geometry. The result was approximately

$$P_2 = C\left[\beta_p(R) + \beta_m(R) + \beta_a(R)\right] \tag{2}$$

The program then calculated

$$p = \beta_p(R) / \left[\beta_m + \beta_a\right] \tag{3}$$

by using the signal in the near region to determine the average value of $\beta_m + \beta_a$. The calibration constant disappears in (3), so there was no need to calibrate the lidar.

The data in polar coordinates (range and elevation angle) were interpolated to a rectangular grid (height above ground and horizontal distance from the lidar) and digital and graphical output generated (Fig. 4). A simple match of a two-dimensional Gaussian was made to each gridded sweep, from which the plume rise and vertical and horizontal dispersion parameters were calculated. The turbulent growth and rise is a random process, so the sweep with the second-highest rise was selected for each aircraft and used to conservatively define "final" plume rise and dispersion for that takeoff.

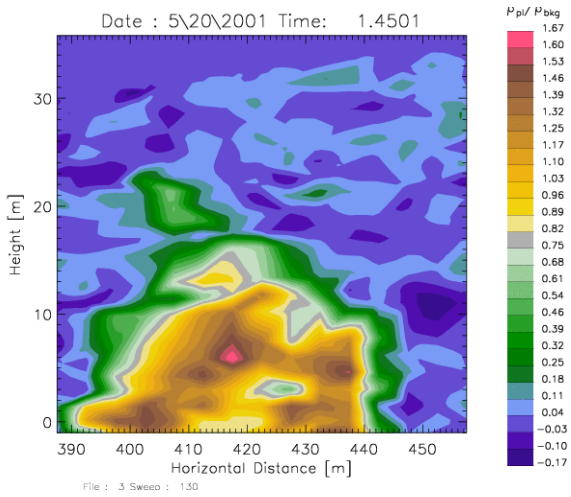

Fig. 4. Example of gridded plume backscatter expressed as a ratio to ambient backscatter.

Statistical analyses were performed for various factors that might affect plume behavior, such as size of aircraft, fuselage- or wing-mounted engines, and atmospheric stability. Although the results suggested trends due to some of these factors, most were not statistically significant in the current data set. For example, atmospheric stability will likely reduce plume rise and vertical dispersion, but there were few samples under such conditions. Horizontal plume size tended to be greater for larger aircraft with wing-mounted engines, presumably because of the separation of initial exhaust locations. Importantly (and perhaps surprisingly), the rise and vertical dispersion of exhaust from large

commercial aircraft were only slightly greater than from smaller commuter aircraft, and the differences were statistically insignificant.

Wayson et al. (2003) recommended the following average plume parameters for input to air quality models:

- Plume height above ground: 12 m
- Vertical dispersion coefficient: 4.1 m
- Horizontal dispersion coefficient: 10.5 m

The Emissions and Dispersion Modeling System used by the U.S. Federal Aviation Administration for evaluation of aviation emission sources from proposed airport projects now uses these values, which are larger than assumed before (Hall et al. 2003).

Additional measurements and research should be able to define the effect of various parameters with statistical significance. Measurements in stable conditions will be particularly important.

5. OPTICAL SIGNATURES FROM SOOT

Scattering calculations at 355-nm wavelength allow examination of the potential for lidar estimation of soot particle concentrations and emission rates. The focus is on particle mass rather than number concentration because of the U.S. National Ambient Air Quality standards are in terms of mass. Although there is interest in numbers as well, the correlation of optical parameters with number concentration is very poor. We seek a relationship between soot mass concentration c and the volumetric backscatter or extinction cross section of soot, or β_s and σ_s respectively. The calculations used values for refractive index, density, and size distributions based on reports of other studies. The Rayleigh-Mie code of Bohren and Huffman (1983) was used, which assumes homogeneous, spherical particles. Soot particles usually are not truly homogeneous spheres, so actual scattering and extinction may deviate from these calculations. However, because the particles are highly absorbing and results are normalized to mass, we anticipate the actual optical behavior will not deviate grossly from the calculations.

Horvath (1993) and Marley et al. (2001) summarized a number of earlier values used and measurements of the complex refractive index $n = n_r - n_i$ of soot, elemental carbon, and black carbon. The n of these highly absorbing materials is difficult to measure. Most of these references do not report the density ρ of the carbon in the particles. Soot particles are usually a mixture of carbon with air in proportions that depend on the formation process. Horvath (1993) assumed $n = 2.0 - 1.0i$ for $\rho = 2.25$ g cm^{-3} and assumed a simple mixing rule to obtain $(n_r - 1) = n_i = \rho$ / (2.25 g cm^{-3}) for less dense particles. We used this method for $\rho = 1.00$, 1.25, 1.50, 1.75, 2.00, and 2.25 g cm^{-3}, although values for soot from aircraft jet engines are most likely limited to the low or middle part of this range.

Lidar backscatter for these refractive index values at 355-nm wavelength can be divided into three regimes according to particle size. Particles with diameter d smaller than ≈50 nm are in the Rayleigh regime; those with d larger than ≈200 nm are in the Mie regime; and those with diameters between are in the "first peak" part of the Mie regime. When normalized to particle mass, β and ρ both exhibit some dependence on n at all particle sizes.

In the Rayleigh regime, β_s scales with d^6 or with m^2, where m is the mass of the particle. Extinction in the Rayleigh regime is dominated by absorption, and σ_s scales as d^3 so that σ_s is proportional to particle mass if ρ is constant.

For $d > 200$ nm in the Mie regime, both scattering and absorption are significant in σ_s. The extinction coefficient depends almost entirely on the cross-sectional area of the particle independent of refractive index, σ_s scales as d^2 irrespective of ρ. The behavior of β_s in this regime is more complicated, exhibiting a damped oscillation as d increases. When the oscillations are smoothed by a running average in d, then β_s increases as d^2 or as $m^{2/3}$ when ρ is held constant.

In the "first peak" part of the Mie regime, β_s normalized to particle mass peaks at about $d = 115$ nm. Scattering becomes important in σ_s as d increases above 50 nm, and σ_s normalized by particle mass peaks at $d \approx 150$ nm.

D. W. Fahey and U. Schumann (in IPCC 1999 pp. 72-76) summarize earlier *in situ* measurements of number size distributions of soot from jet engines, including those of Hagen et al. (1992, 1996) and Petzold et al. (1999). More recent measurements were reported by Petzold et al. (2003) and Nyeki et al. (2004). The size distributions are usually lognormal in shape with count geometrical mean diameters (*CGMD*) of typically 35 nm but ranging over 20-60 nm. The geometric standard deviations (*GSD*) are typically 1.65 but range over 1.55 - 1.72. In this study we use the corresponding mass distributions, which are lognormal with the same *GSD*, but with mass geometrical mean diameters (*MGMD*) typically 70 nm but ranging over 40-120 nm.

The β_s and σ_s were calculated for combinations of *MGMD*, *GSD*, and n and, using the corresponding value of ρ, normalized to c. The dependence on *GSD* was much weaker than on *MGMD* and n, so we show here only results for *GSD* = 1.65.

The β_s / c results for lidar backscatter are shown in Fig. 5. Ideally, β_s / c would be independent of *MGMD* and n, so β_s measured by lidar would reveal the mass concentration c independent of size distribution or refractive index. The dependence on *MGMD* is relatively weak over *MGMD* = 100 ± 25 nm. However, β_s / c decreases significantly outside these limits, especially as *MGMD* becomes smaller. This indicates that separate information about *MGMD* must be obtained for accurate estimation of c from measurements of β_s. A functional relationship between EI_m and *MGMD* may well exist, which might be ascertained with limited *in situ* measurement and applied in the analysis of lidar data. The dependence on n is smaller than on *MGMD* and would become a relatively minor source of error if the appropriate values of n and corresponding ρ can be established for jet engine exhaust.

The dependence of σ_s /c on *MGMD* (Fig. 6) is much less than it is for β_s /c. σ_s also depends on n somewhat less than β_s does. If σ_s can be measured in jet exhaust plumes with accuracy comparable to β_s, it would be a superior method.

The lidar ratios σ_s/β_s for these size distributions are shown in Fig. 7. Especially noteworthy is the accelerating increase in σ_s/β_s as d decreases below 60 nm. This suggests that simultaneous measurement of σ_s and β_s from the jet exhaust could reveal small *MGMD* with an accuracy limited by knowledge of n and measurement accuracy. Another possibility for lidar measurement of small *MGMD* is simultaneous measurement of backscatter at two separate wavelengths. If the refractive index is the same at both wavelengths (a good approximation), then the curves in Fig. 5 shift along the horizontal axis in proportion to the difference from 355 nm. The feasibility of using two wavelengths and of measuring σ_s/β_s for providing information on *MGMD* should both be explored if lidar is to be used extensively for measurement of soot emission rates.

If β_s is to be measured, the lidar must be calibrated to obtain the value of C. Standard methods can be employed to achieve this calibration. For measurement of σ_s, a calibration is not required. A method that can be applied to measure plume extinction (Eberhard et al. 1987) is to first account for extinction in the ambient air by adjusting σ_a to make P in (1) constant in range in approximately homogeneous ambient conditions. The ratio of backscatter from the ambient air on opposite sides (near and far) of the plume provides the optical depth through the plume. With an assumption of constant extinction-to-backscatter ratio, the extinction coefficient along the lidar beam in the plume region can be calculated.

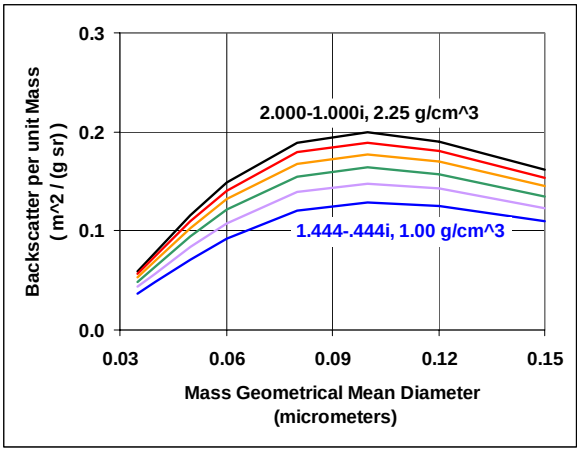

Fig. 5. Lidar backscatter per unit mass β_s /c at 355-nm wavelength versus *MGMD* for lognormal size distributions of spherical soot particles with *GSD* = 1.65 at the indicated values of refractive index n and density of the particles (in g cm^{-3}). The unlabeled curves are for steps in density of 0.25 g cm^{-3} and corresponding change in n.

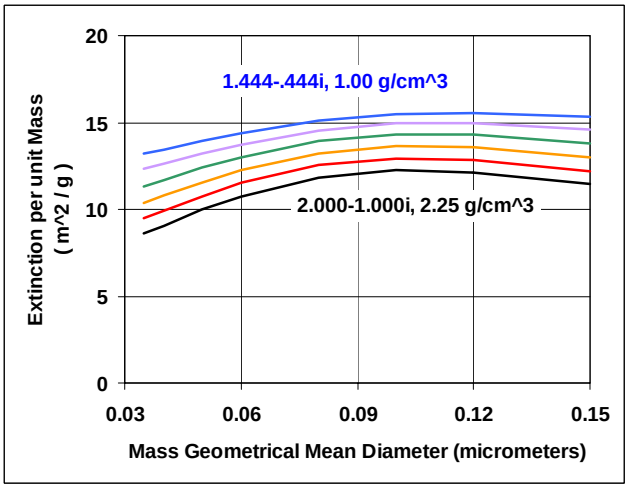

Fig. 6. As in Fig. 5 except for extinction σ_s /c

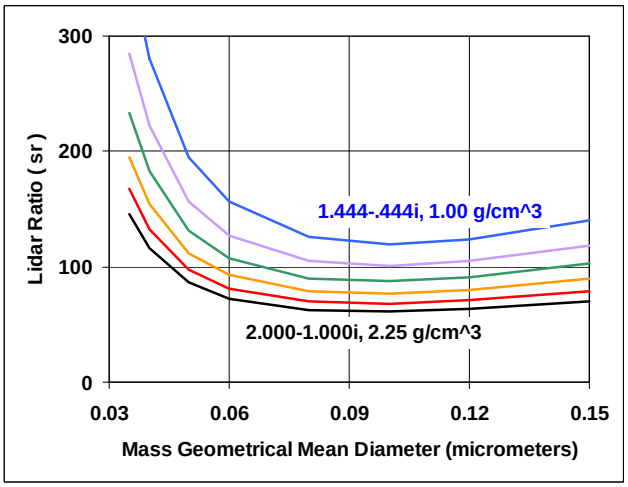

Fig. 7. As in Fig. 6 except for lidar extinction-to-backscatter ratio σ_s / β_s.

6. CONCENTRATION IN EXHAUST CORE

Next to be considered are lidar sampling strategies to obtain soot emission rates from measurements of c. One approach would be to measure $\beta_s = \beta_p$ in the core of the exhaust from the combustor. The fuel consumption rate and air-to-fuel mixture are usually quite well known for each engine's operating configuration. Combining these with concentrations inferred from the lidar data would yield the mass emission index EI_m, i.e., the fraction by mass of fuel converted to soot. The density of the air in the core should be considered as well, for it determines β_m, which must be subtracted to isolate the backscatter from the particles.

If extinction is large enough, it might be determined by measuring backscatter in range gates on either side of the exhaust to obtain the optical depth across the plume.

Measurement of concentrations in the core will place heavy demands on the design of the lidar. The exhaust must be sampled close (<10 m, and perhaps ≈ 1m) behind the nozzle before much turbulent mixing occurs. A range resolution of ≈ 10 cm or finer is desirable to obtain at least one data point only in the core. This would require a special short-pulse laser and very fast detector and digitizer. The transverse resolution should be correspondingly small, which restricts the diameter of the beam and requires high angular precision in pointing or scanning. The limits on resolution might be relaxed if the diameter of the jet exhaust is known independently and the scattering properties of the surrounding air (bypass if a turbofan and ambient air) are known. The coarser the spatial resolution, the larger are the uncertainties in the accounting for these factors. The proximity of the aircraft structure (wings and fuselage) imposes limits on how much the lidar's spatial resolution can be expanded for core measurements.

7. FLUX AND EMISSION RATE

Another approach would be to scan the lidar in elevation angle, as was done for plume geometry, to determine the flux of soot through the plane of the scan. The flux is given by:

$$F = \int_{y,z} c(y,z)\ \mathbf{v}(y,z)\cdot\mathbf{i}\ dydz \qquad (4)$$

where y and z are coordinates in the plane, c is the mass concentration of soot, $\boldsymbol{v}$ is the velocity vector of air moving the soot, and $\boldsymbol{i}$ is the unit vector normal to the flat scan plane with $\boldsymbol{i}$ pointed to the side opposite the aircraft. If θ is the angle between the wind direction and the plane's surface, then $\boldsymbol{v}\cdot\boldsymbol{i} = v\sin\theta$, where v is the speed of the air. For a static aircraft and assuming no change in soot particles between emission and measurement, $F = Q$, where Q is the emission rate.

If the aircraft is moving with velocity $\boldsymbol{V}$, the concentration of particles in the air changes, and the relationship between emission rate and flux measurement becomes

$$Q = \int_{y,z} \left[1 - \frac{\mathbf{V}\cdot\mathbf{j}}{v}\right] c(y,z)\,\mathbf{v}(y,z)\cdot\mathbf{i}\ dydz \qquad (5)$$

where $\boldsymbol{j}$ is the unit vector of wind direction, i.e., $\boldsymbol{j} = \boldsymbol{v}/v$. In this expression $\boldsymbol{V}$ is for the time of emission, so if $\boldsymbol{V}$ is changing due to aircraft acceleration, the transport time from emission to the scan plane should be considered for best accuracy in $\boldsymbol{V}$.

$c(x,y)$ could be inferred from lidar profiles of β_p. Because of mixing with bypass and ambient air, β_p and β_s aren't necessarily identical. Described below are schemes to account for the difference and also to obtain $\boldsymbol{v}$.

7.1 Flux in dynamic exhaust plume

One location a lidar could scan for flux measurement is in a plane roughly perpendicular to the aircraft heading and within a few hundred meters behind the aircraft, where the exhaust is still dynamic. The following additional information is required to complete the flux measurement:

1) the profile of exhaust velocity $\boldsymbol{v}(x,y)$ over the scan plane, which could be obtained by measurements or models. The use of models confirmed by measurements would be the most practical. Models have been developed to describe the safety environment for ground operations (e.g. at www.boeing.com). For our purpose, models should consider the type of engine and aircraft, power setting, aircraft speed, and the ambient wind.

2) the profile of air temperature $T(x,y)$ in the plume over the scan plane. This is needed to determine the density of the air to calculate a correct β_m and σ_m . Modeling supported by measurements, analogous to that for exhaust velocity, would seem to be the best approach.

3) the contribution to backscatter or extinction in the exhaust plume caused by mixing of particles in the ambient air into the plume. It is reasonable to assume that particles ingested into the combustor are volatized. The fate of ambient particles in the bypass air is less obvious and would need to be understood. Models used for #1 might provide the amount of mixing. The plume dimensions measured by the lidar would provide an independent check for consistency. The higher the EI_m and the lower β_p,, the less need for accuracy in understanding the fate of the ambient particles.

7.2 Flux by transport in the ambient wind

The complications of #1 and #2 in Sec. 7.1 could be eliminated by scanning the lidar farther away from the aircraft where the exhaust dynamics have decayed and the ambient wind transports the plume. Then $\boldsymbol{v}$ is the same as the ambient wind, which can be easily measured. Temperature enhancement in the plume at such distances would be insignificant. However, understanding the degree of mixing with ambient air will be important.

Changing the orientation of the scan plane may be optimum for measuring emission rates, especially if observation of extinction is part of the strategy. Consider orienting the scan roughly parallel to the runway and offset on the downwind side. As aircraft take off, the plume will drift almost sideways through the scan plane unless the wind direction is almost exactly parallel to the scan plane. The high exhaust velocities will decay away before reaching the scan plane, or at least will be much less important because they are approximately parallel to it. The path length of the lidar beam through the plume will be much greater than for perpendicular scans, so the plume's optical depth will be larger and easier to measure. The degree of mixing of ambient air could be evaluated by comparing the plume volume measured by the lidar to the volume of air passing through the engine. Although scans roughly perpendicular to the plume's direction of movement are best for measuring plume geometry, a nearly parallel geometry could be far superior for measuring emission rates.

8. CONCLUSIONS

A lidar operating at 355-nm wavelength was safely able to measure the geometry of exhaust plumes from a wide variety of commercial jet aircraft. Data from that experiment have been used to improve an air quality forecast model. Additional measurements would be required to increase the statistical data sample to determine the dependence of initial plume rise and dispersion on aircraft thrust, the location of the engines, and atmospheric stability.

Anecdotal evidence from the plume geometry measurements and simulations of backscatter and extinction in this paper indicate that an ultraviolet lidar could also measure concentrations of soot in the exhaust plume and use sampling strategies with auxiliary information to infer the mass emission rates from the engines. A more definitive understanding of each of the following would improve the accuracy of emission rate measurements:

1) density and refractive index of soot particles from aircraft jet engines, both primary and aggregated;
2) rate and amount of deposition of plume constituents such as hydrocarbons and sulfuric acid on the soot particles;
3) effect of nonspherical particles on backscatter and extinction;
4) for flux measurements in the dynamic plume, verified models that give the velocity and temperature structure of the plume and amount of mixing of ambient air;
5) and, for flux measurements by transport by the ambient wind, evaluation of how much ambient air is mixed into the exhaust from the engine.

Mass emission rates from jet engines during airport operations are currently known only within a factor of a few, so high accuracy is not necessary for such measurements to be useful.

Lidar scattering from ambient particles is a source of interference that can be accounted for, at least to some extent. However, future observations would benefit from a location and time when concentrations of ambient particles are low, i.e., when visual range is large.

One important advantage of lidar for measuring jet exhaust is that data can be acquired remotely during real-life conditions. The measurements are entirely noninvasive and do not interfere with airport operations. Lidar can sample a large number and variety of aircraft with relative ease to examine how exhaust characteristics vary among types of aircraft.

Acknowledgments

Thanks to Los Angeles World Airports (LAWA) and the FAA and DOT for funding support. Julie Draper of FAA and Gregg Fleming of DOT provided important encouragement and assistance. Valuable help for the plume geometry project was provided by Bob Holden of LAWA, John Pehrson of Camp Dresser & McKee Inc., and Richard Marchbanks, Ann Weickmann, Joanne George, and Christoph Senff of the Environmental Technology Laboratory.

REFERENCES

Bohren, C. F, and D. R. Huffman, 1983: *Absorption and Scattering of Light by Small Particles.* Wiley 530 pp.

Eberhard, W. L., G. T. McNice, and S. W. Troxel, 1987: Lidar sensing of plume dispersion: Analysis methods and product quality for light-scattering tracer particles. *J. Atmos Oceanic Technol.*, **4**, 674-689.

Hall, C. T., T. G. Thrasher, J. A. Draper, C. A. Holsclaw, R. L. Wayson, B. Y. Kim, and G. G. Fleming, 2003: FAA EDMS airport air quality model development. *Proceedings, 96th Ann. Mtg. AWMA*, San Diego, CA, Air and Waste Management Assoc., #69574.

Hagen, D. E., M. B. Trueblood, and P. D. Whitefield, 1992: A field sampling of jet exhaust aerosols. *Part. Sci. Technol.*, **10**, 53.

Hagen, D. E., P. D. Whitefield, and H. Schlager, 1996: Particulate emissions in the exhaust plume from commercial jet aircraft under cruise conditions. *J. Geophys. Res.*, **101**, 19,551-19,557.

IPCC (Intergovernmental Panel on Climate Change), 1999: *Aviation and the Global Atmosphere*, Cambridge University Press, 373 pp.

Horvath, H., 1993: Atmospheric light absorption – a review. *Atmos. Env.*, **27A**, 293-317.

Marley, N. A., J. S. Gaffney, J. C. Baird, C. A. Blazer, P. J. Drayton, and J. E. Frederick, 2001: An empirical method for determination of the complex refractive index of size-fractionated atmospheric aerosols for radiative transfer calculations. *Aerosol Sci. Technol.*, **34**, 535-549.

Nyeki, S., M. Gysel, E. Weingartner, U. Baltensperger, R. Hitzenberger, A. Petzold, and C. W. Wilson, 2004: Properties of jet engine combustion particles during the PartEmis experiment: Particle size spectra (d>15 nm) and volatility. *Geophys. Res. Let.*, **31**, L18105.

Petzold, A., A. Döpelheuer, C. A. Brock, and F. Schröder, 1999: In situ observations and model calculations of black carbon emission by aircraft at cruise altitude. *J. Geophys. Res.*, **104**, 22,171-22,181.

Petzold, A., C. Stein, S. Nyeki, M. Gysel, E. Weingartner, U. Baltensperger, H. Giebl, R. Hitzenberger, A. Döpelheuer, S. Vrchoticky, H. Puxbaum, M. Johnson, C. D. Hurley, R. Marsh, and C. W. Wilson, 2003: Properties of jet engine combustion particles during the PartEmis experiment: Microphysics and chemistry. *Geophys. Res. Let.*, **30**, 1719.

Wayson, R. L., G.G. Fleming, B. Kim, W. L. Eberhard, W. A. Brewer, J. Draper, J. Pehrson and R. Johnson, 2003: The use of lidar to characterize aircraft exhaust plumes. *Proceedings, 96th Ann. Mtg. AWMA*, San Diego, CA, Air and Waste Management Assoc., #69965.